

Published in final edited form as:

Neuron. 2014 March 5; 81(5): 1084–1096. doi:10.1016/j.neuron.2014.01.035.

Distinct functional and pharmacological properties of triheteromeric GluN1/GluN2A/GluN2B NMDA receptors

Kasper B. Hansen^{1,2}, Kevin K. Ogden¹, Hongjie Yuan¹, and Stephen F. Traynelis¹

¹Department of Pharmacology, Emory University School of Medicine, Atlanta, Georgia, 30322, USA

Summary

NMDA receptors are tetrameric ligand-gated ion channels comprised of GluN1, GluN2, and GluN3 subunits. Two different GluN2 subunits have been identified in most NMDA receptor-expressing cells, and the majority of native receptors are triheteromers containing two GluN1 and two different GluN2. In contrast to diheteromeric NMDA receptors, little is known about the function of triheteromers. We developed a method to provide selective cell-surface expression of recombinant GluN1/GluN2A/GluN2B triheteromers, and compared properties of these receptors with those of GluN1/GluN2A and GluN1/GluN2B diheteromers. We show that glutamate deactivation of triheteromers is distinct from those of GluN1/GluN2A and GluN1/GluN2B, and reveal modulation of triheteromers by subunit-selective antagonists ifenprodil, CP-101,606, TCN-201, and extracellular Zn²⁺. Furthermore, kinetic measurements suggest variation in the ifenprodil binding site of triheteromers compared to GluN1/GluN2B diheteromers. This work provides new insight to the distinct properties of GluN1/GluN2A/GluN2B triheteromers, which are presumably the most abundant NMDA receptors in the adult forebrain.

Introduction

NMDA receptors are ionotropic glutamate receptors that are critically involved in many processes in the central nervous system (CNS), including neuronal development, memory, and learning (Traynelis et al., 2010). However, they are also implicated in a multitude of psychiatric and neurological disorders, such as schizophrenia, depression, epilepsy, stroke, and traumatic brain injury, as well as Parkinson's, Huntington's, and Alzheimer's diseases (Paoletti et al., 2013; Traynelis et al., 2010). NMDA receptors are therefore widely considered as important targets for therapeutic intervention in many diseases of the CNS.

Seven NMDA receptor subunits have been cloned: GluN1, GluN2A-D, and GluN3A-B. The majority of native NMDA receptors are tetrameric assemblies of two GluN1 subunits and two GluN2 subunits (Traynelis et al., 2010). GluN3 can also assemble with GluN1 and GluN2, but the stoichiometry of GluN3-containing receptors is unknown. Studies on recombinant NMDA receptors almost exclusively describe diheteromeric receptors that are assembled from GluN1 and only one type of GluN2. However, at least two different GluN2 subunits have been identified in most, if not all, NMDA receptor-expressing cells.

© 2014 Elsevier Inc. All rights reserved.

Correspondence: Kasper B. Hansen (kasper.hansen@mso.umt.edu).

²Present address: Department of Biomedical and Pharmaceutical Sciences, University of Montana, Missoula, Montana, 59812, USA.

Publisher's Disclaimer: This is a PDF file of an unedited manuscript that has been accepted for publication. As a service to our customers we are providing this early version of the manuscript. The manuscript will undergo copyediting, typesetting, and review of the resulting proof before it is published in its final citable form. Please note that during the production process errors may be discovered which could affect the content, and all legal disclaimers that apply to the journal pertain.

Furthermore, a compelling body of evidence shows that a large proportion of native NMDA receptors are triheteromers assembled from two GluN1 and two different GluN2 subunits. In particular, it has been demonstrated that GluN1/GluN2A/GluN2B triheteromers account for >50% of the total NMDA receptors in hippocampus and cortex of the adult rodent brain (Al-Hallaq et al., 2007; Luo et al., 1997; Rauner and Kohr, 2011; Sheng et al., 1994; Tovar et al., 2013); but see also (Chazot and Stephenson, 1997). Despite the prevalence of triheteromeric NMDA receptors *in vivo*, there is a fundamental gap in our knowledge of their function and pharmacology due to our inability to faithfully express these triheteromeric receptors in heterologous expression systems without accompanying diheteromeric receptors (Chazot et al., 1994; Hatton and Paoletti, 2005; Tovar and Westbrook, 1999; Vicini et al., 1998).

Co-expression of GluN1 with two different GluN2 subunits (e.g. GluN2A and GluN2B) in heterologous systems generates three populations of functional NMDA receptors consisting of two different diheteromeric receptors (e.g. GluN1/GluN2A and GluN1/GluN2B) as well as triheteromeric receptors (e.g. GluN1/GluN2A/GluN2B). Expression of three receptor populations confounds studies on the properties of triheteromeric receptors. To mitigate this problem, we exploited the trafficking control system of the G protein-coupled GABA_B receptors that are heterodimers composed of GABA_{B1} and GABA_{B2} subunits (Bettler et al., 2004). The GABA_{B1} subunit possesses a retention signal (RXR motif) in the intracellular C-terminal domain (CTD) that retains the subunit in the endoplasmic reticulum (ER) and thus prevents expression of homomeric GABA_{B1} at the cell surface (Margeta-Mitrovic et al., 2000). However, the retention signal is masked through a coiled-coil interaction with GABA_{B2} between leucine zipper motifs within in the CTDs, allowing trafficking of the heterodimer to the cell surface (Margeta-Mitrovic et al., 2000). With some modifications, the GABA_B receptor trafficking system has been utilized to express heterodimeric metabotropic glutamate receptors in heterologous systems upon transfer of the intracellular GABA_B subunit CTDs (Kniazeff et al., 2004).

We took advantage of the GABA_B receptor leucine zipper motifs and engineered C-terminal peptide tags that were used to selectively express recombinant triheteromeric receptors at the cell-surface without confounding co-expression of diheteromeric receptors. Thus, this approach enables quantitative evaluation of functional and pharmacological properties of GluN1/GluN2A/GluN2B triheteromeric receptors.

Results

Selective cell-surface expression of triheteromeric GluN1/GluN2A/GluN2B receptors

In order to selectively express triheteromeric NMDA receptors at the cell-surface, we engineered two different C-terminal peptide tags composed of the leucine zipper motifs from GABA_{B1} and GABA_{B2} (LZ1 and LZ2, respectively) immediately followed by C-terminal dilysine KKXX ER retention/retrieval motifs (Figure 1A and Figure S1). The leucine zipper motifs of GABA_{B1} and GABA_{B2} can interact to form a parallel heterodimeric coiled-coil structure (Kammerer et al., 1999). The KKXX motifs at the distal C-termini will localize the subunits in the ER (Zerangue et al., 2001) unless masked by coiled-coil formation between LZ1 and LZ2 (Brock et al., 2005). Finally, we added a peptide linker (L4) to the N-termini to generate the tags L4-LZ1-KKXX and L4-LZ2-KKXX (hereafter denoted C1 and C2, respectively). The L4 peptide linker was composed of four repeats of amino acids EAAAK, which will generate a rigid α -helical rod (Arai et al., 2004). Fusing C1 and C2 to the intracellular C-termini of GluN2 subunits should allow selective surface expression of NMDA receptors composed of two GluN1, one C1-tagged GluN2, and one C2-tagged GluN2 (Figure 1B). To avoid potential incompatibility between trafficking signals present in GluN2A and GluN2B CTDs and between CTD structures and spatial requirements for the C1/C2 interaction, we replaced the CTD of GluN2B with that of

GluN2A (Figure 1A). The functional properties of GluN2B subunits containing the CTD of GluN2A are indistinguishable from those of wild type GluN2B (Maki et al., 2012; Punnakkal et al., 2012). Thus, we generated C1- and C2-tagged GluN2A and GluN2B subunits ($2A_{C1}$, $2A_{C2}$, $2B_{AC1}$, and $2B_{AC2}$) that only differ in the intracellular CTDs by the leucine zipper motifs (LZ1 and LZ2). The amino acid sequences for the C1 and C2 peptide tags are shown in Figure S1.

Co-expression of $2A_{C1}$ and $2B_{AC2}$ (as well as GluN1) in *Xenopus* oocytes produced robust currents responses activated by glutamate plus glycine that increased in amplitude on days 1–3 following cRNA injection and remained constant on days 4–6 (Figure 1C,D). In theory, the glutamate/glycine-activated currents from oocytes co-expressing $2A_{C1}$, $2B_{AC2}$, and GluN1 are mediated by NMDA receptors composed of one $2A_{C1}$ and one $2B_{AC2}$ with masked retention signals, as well as two GluN1 subunits (hereafter referred to as $2A_{C1}/2B_{AC2}$). However, some $2A_{C1}/2A_{C1}$ and $2B_{AC2}/2B_{AC2}$ receptors that may have escaped ER retention could also contribute to the measured current responses. To evaluate the fraction of the total current response that is mediated by escaped receptors (i.e. “escape” current), we generated $2A_{C1}$ and $2B_{AC2}$ subunits with mutations in the agonist binding pocket that abolish glutamate binding (R518K + T690I in $2A_{C1(RK+TI)}$ and R519K + T691I in $2B_{AC2(RK+TI)}$) (Erreger et al., 2007; Hatton and Paoletti, 2005; Laube et al., 1997). Co-expression of $2A_{C1}$ and $2B_{AC2(RK+TI)}$ produces only one population of receptors that can be activated by 100 μ M glutamate, namely escaped $2A_{C1}/2A_{C1}$, since agonist occupancy at two GluN2 subunits are required for NMDA receptor activation (Benveniste and Mayer, 1991; Clements and Westbrook, 1991) (Figure 1C,D). Thus, comparison of current responses from oocytes expressing $2A_{C1}/2B_{AC2}$ with responses from oocytes co-expressing $2A_{C1}/2B_{AC2(RK+TI)}$ allows estimation of the fractional current mediated by escaped $2A_{C1}/2A_{C1}$. Similarly, comparison to current responses from oocytes expressing $2A_{C1(RK+TI)}/2B_{AC2}$ allows estimation of the fractional current mediated by escaped $2B_{AC2}/2B_{AC2}$ (Figure 1C,D). The sum of the fractional currents from escaped $2A_{C1}/2A_{C1}$ and $2B_{AC2}/2B_{AC2}$ assessed using this approach will provide an estimate of the percent “escape” current in oocytes co-expressing $2A_{C1}$ and $2B_{AC2}$ that is mediated by receptors other than triheteromeric $2A_{C1}/2B_{AC2}$. For the $2A_{C1}/2B_{AC2}$ subunit combination, the percent “escape” current was between 3–7% on days 2–4 of expression (5 batches of oocytes, N = 6 oocytes each day for each batch) (Figure 1E). Similar results were obtained for $2A_{C1}/2A_{C2}$ and $2B_{AC1}/2B_{AC2}$ subunit combinations (Figure 1E; see also Figure S1).

To provide an alternative evaluation of the efficiency by which the engineered peptide tags express a homogenous population of triheteromeric receptors, we introduced a mutation in the agonist binding pocket that reduces glutamate potency (H485A in GluN2A and H486A in GluN2B) (Anson et al., 1998; Hansen et al., 2005). If there is observable “escape” current, then glutamate concentration-response data from oocytes co-expressing wild type and mutated subunits will have three components mediated by receptors with one binding site mutated as well as escaped wild type and double-mutant receptors. Thus, this approach will allow evaluation of “escape” current in individual oocytes by assessing the fractional sizes of the components in the glutamate concentration-response data (see Figures S2–S3 and Table S1). The results obtained using this approach to evaluate the efficiency of the peptide tags were consistent with “escape” currents estimated using the “RK+TI” mutations.

In summary, we have engineered peptide tags (C1 and C2) that upon fusion to the C-terminus of GluN2A and GluN2B subunits facilitate selective expression of NMDA receptors with a defined subunit combination at the cell-surface, thereby enabling experiments on a homogenous population of triheteromeric GluN1/GluN2A/GluN2B receptors.

Inhibition of triheteromeric receptors by GluN2A-selective modulators

The lack of information regarding properties of triheteromeric receptors has been a major obstacle in studies using subtype-selective antagonists to assess the physiological roles of native NMDA receptors. Moreover, the inability to study triheteromeric NMDA receptors that are abundant in the adult brain complicates clinical development of subunit-selective modulators. By controlling the subunit composition of cell surface-expressed receptors using the engineered peptide tags we can begin to quantitatively evaluate the activity of subunit-selective modulators at GluN1/GluN2A/GluN2B triheteromers.

We examined the GluN2A-selective antagonist TCN-201, which is a negative allosteric modulator of glycine binding to GluN1 (Bettini et al., 2010; Hansen et al., 2012). The presence of the peptide tags in the CTD did not alter potency and maximal inhibition for TCN-201 at $2A_{C1}/2A_{C2}$ compared to wild type $2A/2A$, and TCN-201 did not display any activity at wild type $2B/2B$ and $2B_{AC1}/2B_{AC2}$ receptors (Figure 2A and Table 1). However, the IC_{50} of TCN-201 increased from 370 ± 30 nM at wild type $2A/2A$ ($N = 8$) to 1350 ± 130 nM at $2A_{C1}/2B_{AC2}$ triheteromers ($N = 10$) and maximal inhibition was reduced from $91 \pm 1\%$ to $72 \pm 4\%$ (Figure 2A and Table 1). Thus, the presence of a single GluN2A subunit in triheteromers reduces TCN-201 inhibition compared to receptors with two GluN2A subunits. TCN-201 inhibition of $2A_{C1}/2B_{AC2}$ and $2A_{C2}/2B_{AC1}$ triheteromers (i.e. the C1- and C2-tags were swapped between the GluN2A and GluN2B subunits) was not significantly different (Figure S4).

Extracellular Zn^{2+} can inhibit NMDA receptors at low nanomolar concentrations in a voltage-independent manner by binding to a high-affinity site in the amino-terminal domain (ATD) of GluN2A (Choi and Lipton, 1999; Paoletti et al., 2000). In addition, Zn^{2+} inhibition can occur through binding to the GluN2B ATD, albeit at higher micromolar concentrations (Karakas et al., 2009; Rachline et al., 2005). Extracellular Zn^{2+} can also produce a non-specific voltage-dependent channel block through binding to the NMDA receptor ion channel pore (Williams, 1996). Despite a significant role of Zn^{2+} as an endogenous NMDA receptor modulator (Nozaki et al., 2011; Sensi et al., 2011), little is known about its actions on GluN1/GluN2A/GluN2B triheteromers. One previous study reported inhibition of triheteromers by extracellular Zn^{2+} in the nanomolar range, but could not provide robust values for potency and efficacy (Hatton and Paoletti, 2005). Since inhibition by extracellular Zn^{2+} is considered relevant for the physiological function of GluN2A-containing NMDA receptors (Sensi et al., 2011), we decided to determine the potency and efficacy at triheteromers. To minimize the voltage-dependent, low-affinity component of Zn^{2+} inhibition, we recorded at a holding potential of -20 mV and Zn^{2+} concentrations were kept below 300 nM. Under these conditions, we did not observe differences between Zn^{2+} inhibition of wild type $2A/2A$ and $2A_{C1}/2A_{C2}$, as well as wild type $2B/2B$ and $2B_{AC1}/2B_{AC2}$, supporting the idea that neither the GluN2A CTD in GluN2B nor the peptide tags change receptor properties (Figure 2B and Table 1). At physiological pH 7.3, Zn^{2+} displayed high-potency inhibition of wild type $2A/2A$ with an IC_{50} value of 61 ± 4 nM and a maximal inhibition of $57 \pm 2\%$ ($N = 18$), consistent with previous reports (Low et al., 2000; Paoletti et al., 1997; Traynelis et al., 1998; Williams, 1996). At a concentration of 265 nM, extracellular Zn^{2+} reduced responses from wild type $2B/2B$ to $80 \pm 1\%$ ($N = 6$) of control (Figure 2B and Table 1), consistent with minimal voltage-dependent channel block and inhibition primarily mediated through binding to the GluN2B ATD (Karakas et al., 2009; Rachline et al., 2005; Traynelis et al., 1998).

The presence of only a single high-affinity GluN2A binding site in the $2A_{C1}/2B_{AC2}$ triheteromers did not change the potency of Zn^{2+} inhibition at physiological pH 7.3 compared to wild type $2A/2A$ (Figure 2D,F,G and Table 1). The IC_{50} of extracellular Zn^{2+} at $2A_{C1}/2B_{AC2}$ triheteromers was 58 ± 2 nM ($N = 28$) compared to 61 ± 4 nM ($N = 18$) at

wild type 2A/2A. However, there was a reduction in the fitted maximal Zn^{2+} inhibition of $2A_{C1}/2B_{AC2}$ triheteromers ($49 \pm 1\%$) compared to wild type 2A/2A ($57 \pm 2\%$). Zn^{2+} inhibition of $2A_{C1}/2B_{AC2}$ and $2A_{C2}/2B_{AC1}$ triheteromers (i.e. the C1- and C2-tags were swapped) was not significantly different (Figure S4). The high-potency and efficacious inhibition of triheteromers by extracellular Zn^{2+} was unexpected and suggest that not only GluN1/GluN2A diheteromers, but also GluN1/GluN2A/GluN2B triheteromers in the adult brain are modulated by endogenous Zn^{2+} .

Binding of Zn^{2+} to the GluN2A ATD increases proton inhibition of the NMDA receptor, and Zn^{2+} binding presumably inhibits the receptor by increasing proton affinity and thereby the fraction of protonated, nonfunctional receptors (Choi and Lipton, 1999; Erreger and Traynelis, 2005, 2008; Low et al., 2000; Traynelis et al., 1998). The functional link between Zn^{2+} and proton inhibition causes the maximal Zn^{2+} inhibition to increase at more acidic pH and diminish at more alkaline pH. We therefore compared Zn^{2+} inhibition of $2A_{C1}/2B_{AC2}$ triheteromers and wild type 2A/2A at more alkaline pH 7.8 and more acidic pH 6.8 (Figure 2C,E and Table 1). Inhibition by Zn^{2+} at alkaline pH 7.8 was indistinguishable for wild type 2A/2A and $2A_{C1}/2B_{AC2}$ triheteromers with IC_{50} values of 62 ± 4 nM ($N = 10$) and 63 ± 7 nM ($N = 10$), respectively, and maximal inhibition of $29 \pm 1\%$ and $30 \pm 1\%$, respectively. By contrast, there were differences between Zn^{2+} inhibition of wild type 2A/2A and $2A_{C1}/2B_{AC2}$ triheteromers at acidic pH 6.8 with IC_{50} values of 47 ± 2 nM ($N = 6$) and 57 ± 5 nM ($N = 10$), respectively, and maximal inhibition of $93 \pm 2\%$ and $65 \pm 1\%$, respectively. These results suggest that although Zn^{2+} binds with high affinity to NMDA receptors with a single GluN2A subunit, binding to a single site in the receptor is not capable of increasing proton inhibition to the same extent as binding to two high-affinity sites as in wild type 2A/2A.

To evaluate whether Zn^{2+} binding to the GluN2B ATD contributes to Zn^{2+} inhibition of $2A_{C1}/2B_{AC2}$ triheteromers, we eliminated Zn^{2+} binding to GluN2B by mutating a key residue in the Zn^{2+} binding site (H127A) (Karakas et al., 2009; Rachline et al., 2005). There was no marked difference between Zn^{2+} inhibition of $2A_{C1}/2B_{AC2}$ and mutated $2A_{C1}/2B_{AC2}(H127A)$ triheteromers with IC_{50} values of 58 ± 2 nM ($N = 28$) and 44 ± 8 nM ($N = 6$), respectively, and maximal inhibition of $49 \pm 1\%$ and $47 \pm 3\%$, respectively (Figure 2H). Since Zn^{2+} binding to GluN2B is not contributing to the inhibition of $2A_{C1}/2B_{AC2}$ triheteromers, we evaluated inhibition of GluN1/GluN2A diheteromers with only a single intact high-affinity site by mutating the putative Zn^{2+} binding site in one GluN2A subunit (i.e. $2A_{C1}/2A_{C2}(H128S)$). By contrast to $2A_{C1}/2B_{AC2}$ triheteromers that contain a single GluN2A subunit, both potency and maximal inhibition by Zn^{2+} were markedly reduced for $2A_{C1}/2A_{C2}(H128S)$ that also possesses a single high-affinity Zn^{2+} binding site (Figure 2H). The IC_{50} for Zn^{2+} inhibition of $2A_{C1}/2A_{C2}(H128S)$ was 120 ± 20 nM and maximal inhibition was $21 \pm 3\%$ ($N = 11$). Extracellular Zn^{2+} did not produce any inhibition of GluN1/GluN2A diheteromers with both high-affinity sites mutated ($2A_{C1}(H128S)/2A_{C2}(H128S)$; $N = 6$), consistent with the absence of voltage-dependent channel block by Zn^{2+} under these experimental conditions (Figure 2H). The results obtained for GluN1/GluN2A diheteromers with a single or both Zn^{2+} binding sites mutated are consistent with previous reports (Hatton and Paoletti, 2005; Nozaki et al., 2011; Paoletti et al., 2000). However, the similar Zn^{2+} inhibition of GluN1/GluN2A/GluN2B triheteromers and GluN1/GluN2A diheteromers is unexpected when contrasted with the reduced Zn^{2+} inhibition of $2A_{C1}/2A_{C1}(H128S)$, and invites additional experiments to fully delineate the mechanism of Zn^{2+} modulation.

Inhibition of triheteromeric receptors by GluN2B-selective modulators

Non-competitive antagonists that selectively bind at the interface between GluN1 and GluN2B ATDs (Burger et al., 2012; Karakas et al., 2011), such as ifenprodil and CP-101,606, have been extensively explored in the treatment of several neuropathological

conditions (Traynelis et al., 2010). Recently, these antagonists have received renewed interest following the discovery that CP-101,606 is effective against treatment-resistant depression (Preskorn et al., 2008). Despite the considerable resources used in the development of GluN2B-selective antagonists as therapeutic agents, there is a problematic lack of information regarding the activity of these ligands at GluN1/GluN2A/GluN2B triheteromers.

We therefore compared ifenprodil inhibition of triheteromers to that of GluN1/GluN2A and GluN1/GluN2B diheteromers. We recorded at a holding potential of -40 mV to minimize non-specific voltage-dependent inhibition by ifenprodil, which is pronounced at concentrations above 3 μ M (Figure S5). Ifenprodil reduced current responses from wild type 2B/2B with an IC_{50} of 72 ± 8 nM and maximal inhibition of $88 \pm 2\%$ ($N = 8$), whereas responses from wild type 2A/2A were insensitive to 3 μ M ifenprodil ($N = 10$) (Figure 3A,B and Table 1). Ifenprodil inhibition of $2A_{C1}/2B_{AC2}$ triheteromers was markedly reduced compared to wild type 2B/2B, since IC_{50} increased 6.3-fold to 450 ± 30 nM and maximal inhibition was $32 \pm 1\%$ ($N = 16$). Ifenprodil inhibition of $2A_{C1}/2B_{AC2}$ and $2A_{C2}/2B_{AC1}$ triheteromers (i.e. the C1- and C2-tags were swapped) was not significantly different (Figure S4). Thus, the reduced ifenprodil inhibition of triheteromers compared to wild type 2B/2B is in stark contrast to the virtually unchanged Zn^{2+} inhibition of triheteromers compared to wild type 2A/2A (Table 1). Studies have suggested two populations of ifenprodil-sensitive NMDA receptors in the adult rodent forebrain that have been attributed to GluN1/GluN2B diheteromers with high sensitivity and GluN1/GluN2A/GluN2B triheteromers with lower sensitivity (Gray et al., 2011; Kew et al., 1998; Tovar and Westbrook, 1999). Our ability to quantitatively evaluate the pharmacology of triheteromers conclusively validate this idea and also demonstrate that reduced ifenprodil sensitivity of triheteromers is mainly mediated by a diminished maximal inhibition rather than a dramatic reduction in potency (Figure 3A,B and Table 1).

To assess whether our findings regarding ifenprodil inhibition of triheteromers can transfer to other GluN2B-selective antagonists, we also evaluated CP-101,606. Responses from wild type 2B/2B was inhibited by CP-101,606 with an IC_{50} of 61 ± 3 nM and maximal inhibition of $89 \pm 1\%$ ($N = 8$), whereas responses from wild type 2A/2A were insensitive to 3 μ M CP-101,606 ($N = 10$) (Figure 3C and Table 1). CP-101,606 inhibition of $2A_{C1}/2B_{AC2}$ triheteromers had a maximal inhibition of $29 \pm 2\%$ and an IC_{50} of 220 ± 20 nM ($N = 9$), which is increased 3.6-fold compared to wild type 2B/2B. Thus, the presence of a single GluN2B subunit in $2A_{C1}/2B_{AC2}$ triheteromers has a quantitatively similar outcome for inhibition by ifenprodil and CP-101,606 (Figure 3B,C and Table 1).

It has been shown previously that inhibition of triheteromers by a high concentration of ifenprodil is enhanced by the presence of extracellular Zn^{2+} , presumably through Zn^{2+} binding to the single high-affinity site in the GluN2A ATD (Hatton and Paoletti, 2005). To study this observation in more detail, we generated ifenprodil and CP-101,606 concentration-response data in the presence of 300 nM Zn^{2+} . The presence of extracellular Zn^{2+} resulted in a slight increase in both ifenprodil and CP-101,606 potencies at wild type 2B/2B without affecting maximal inhibition (Figure 3D,E and Table 1), whereas wild type 2A/2A remained insensitive to both ifenprodil ($N = 10$) and CP-101,606 ($N = 10$). Ifenprodil and CP-101,606 potencies were slightly increased at $2A_{C1}/2B_{AC2}$ triheteromers by the presence of extracellular Zn^{2+} , whereas a more pronounced effect on maximal inhibition could be observed. Maximal ifenprodil inhibition increased from $32 \pm 1\%$ ($N = 16$) in the absence of Zn^{2+} to $50 \pm 2\%$ ($N = 8$) in the presence of Zn^{2+} , and maximal CP-101,606 inhibition increased from $29 \pm 2\%$ ($N = 9$) to $58 \pm 2\%$ ($N = 8$) (Figure 3D,E and Table 1). This finding is highly relevant to the application of GluN2B-selective antagonists as pharmacological tools or therapeutic agents, because tonic or synaptic Zn^{2+} have been

suggested to be present during electrophysiological recordings and in normal brain physiology (Paoletti et al., 1997; Sensi et al., 2011; Traynelis et al., 1998).

Time-course of ifenprodil inhibition of GluN1/GluN2A/GluN2B receptors

In order to investigate the nature of the ifenprodil binding site in GluN1/GluN2A/GluN2B triheteromers, we evaluated the kinetics of ifenprodil inhibition using fast-application whole-cell patch-clamp recordings. For this purpose, we first optimized the engineered peptide tags to control subunit composition of NMDA receptors expressed in HEK293 cells (see Experimental Procedures). Initially, we measured the time course and concentration-dependence of ifenprodil inhibition of steady-state responses from wild type 2B/2B (Figure 4A). The onset of ifenprodil inhibition of wild type 2B/2B was adequately described by a single exponential function to obtain the inhibition time constants ($\tau_{\text{inhibition}}$). Furthermore, $1/\tau_{\text{inhibition}}$ was linearly related to the concentration of ifenprodil (Figure 4C), which is consistent with a simple bimolecular reaction. The slope of the linear fit to this relationship therefore provides the rate of ifenprodil binding (k_{on}), which was $0.263 \mu\text{M}^{-1}\cdot\text{s}^{-1}$ for wild type 2B/2B (95% confidence interval was $0.236\text{--}0.290 \mu\text{M}^{-1}\cdot\text{s}^{-1}$; $N = 6$). Assuming that unbinding is concentration-independent, the rate of ifenprodil unbinding (k_{off}) derived from the y-intercept was 0.096 s^{-1} (95% confidence interval was $0.051\text{--}0.141 \text{ s}^{-1}$). Thus, the $K_{\text{d}} = k_{\text{off}}/k_{\text{on}}$ for ifenprodil binding to wild type 2B/2B was 370 nM, which is similar to the K_{d} of 320 nM measured using isothermal titration calorimetry with purified GluN1 and GluN2B ATDs (Karakas et al., 2011).

We next measured the kinetics of ifenprodil inhibition of steady-state responses from $2A_{\text{C1}}/2B_{\text{AC2}}$ triheteromers (Figure 4B). Again, the onset of ifenprodil inhibition could be described by a single exponential function, and $1/\tau_{\text{inhibition}}$ was linearly related to the concentration of ifenprodil (Figure 4C). The rate of ifenprodil binding (k_{on}) was $0.099 \mu\text{M}^{-1}\cdot\text{s}^{-1}$ for $2A_{\text{C1}}/2B_{\text{AC2}}$ triheteromers (95% confidence interval was $0.067\text{--}0.131 \mu\text{M}^{-1}\cdot\text{s}^{-1}$; $N = 6$), which was markedly reduced compared to wild type 2B/2B. The rate of ifenprodil unbinding (k_{off}) derived from the y-intercept was 0.065 s^{-1} (95% confidence interval was $0.012\text{--}0.119 \text{ s}^{-1}$). The K_{d} for ifenprodil binding to $2A_{\text{C1}}/2B_{\text{AC2}}$ triheteromers was 660 nM, which is increased 1.8-fold compared to wild type 2B/2B. These results demonstrate that in HEK293 cells expressing $2A_{\text{C1}}/2B_{\text{AC2}}$ triheteromers, the kinetics of ifenprodil inhibition are clearly distinct from those of wild type 2B/2B. In addition, the inhibition by $2.5 \mu\text{M}$ ifenprodil was $36 \pm 1\%$ ($N = 6$) in HEK293 cells expressing $2A_{\text{C1}}/2B_{\text{AC2}}$ triheteromers, which is similar to the maximal inhibition observed in *Xenopus* oocytes ($32 \pm 1\%$; Table 1). The findings that ifenprodil has a markedly slower rate of inhibition, as well as reduced binding affinity and efficacy at GluN1/GluN2A/GluN2B triheteromers compared to GluN1/GluN2B diheteromers suggest structural variation between the ifenprodil binding sites of triheteromeric and diheteromeric GluN2B-containing NMDA receptors.

Deactivation time course for GluN1/GluN2A/GluN2B receptors

GluN2A and GluN2B subunits play distinct physiological roles in many processes of the central nervous system (Paoletti et al., 2013). GluN2B is highly expressed early in development, whereas expression of GluN2A increases during development (Sanz-Clemente et al., 2013). This developmental shift in the relative expression level of these subunits is accompanied by a profound change in pharmacological and functional properties of NMDA receptors. One prominent functional difference is the deactivation time course, which defines the time course of the excitatory postsynaptic current (Lester et al., 1990). The time course of deactivation is in the tens-of-millisecond range for GluN1/GluN2A diheteromers and in the hundreds-of-millisecond range for GluN1/GluN2B (Vicini et al., 1998). However, the deactivation kinetics of NMDA receptor EPSCs in hippocampal and cortical neurons

from adult rodents cannot be explained by a mixture of GluN1/GluN2A and GluN1/GluN2B diheteromers, suggesting that GluN1/GluN2A/GluN2B triheteromers exist in these neurons with distinct and intermediate deactivation kinetics (Gray et al., 2011; Rauner and Kohr, 2011; Tovar et al., 2013).

We directly measured the deactivation time course following removal of glutamate for triheteromeric and diheteromeric NMDA receptors expressed in HEK293 cells using fastapplication whole-cell patch-clamp recordings. Initially, we compared the deactivation kinetics following brief (5 ms) pulses of a supersaturating concentration of glutamate (1 mM) in the continuous presence of glycine (100 μ M). For all receptors, the deactivation time course was adequately described by a double exponential function to obtain time constants for fast and slow components (τ_{fast} and τ_{slow}), and the weighted time constant ($\tau_{weighted}$) could be calculated using the relative contribution from each of these components (Table 2). Consistent with the concentration-response data, neither the presence of the peptide tags nor the GluN2A CTD in GluN2B changed receptor function, since $\tau_{weighted}$ was not significantly different between wild type 2A/2A and 2A_{AC1}/2A_{AC2}, or between wild type 2B/2B and 2B_{AC1}/2B_{AC2} (unpaired t test; two-tailed, $P > 0.05$) (Table 2). The $\tau_{weighted}$ for glutamate deactivation of wild type 2A/2A (32 ± 1 ms; $N = 11$) was approximately 10-fold smaller than the corresponding $\tau_{weighted}$ of wild type 2B/2B (314 ± 13 ms; $N = 15$) (Figure 4D,E and Table 2). For 2A_{AC1}/2B_{AC2} triheteromers, $\tau_{weighted}$ was 57 ± 4 ms ($N = 17$), which is significantly different from $\tau_{weighted}$ values of both wild type 2A/2A and 2B/2B (unpaired t test; two-tailed, $P < 0.05$) (Figure 4D,E and Table 2). Similar results were obtained for all subunit combinations following longer glutamate application (2 s) (Figure S6 and Table S2). Thus, we demonstrate that the presence of a single GluN2A results in a striking acceleration of glutamate deactivation that endows GluN1/GluN2A/GluN2B triheteromers with a distinct and intermediate deactivation time course compared to both GluN1/GluN2A and GluN1/GluN2B diheteromers.

In addition to reducing the response amplitude, it has been demonstrated that binding of extracellular Zn^{2+} to GluN2A or ifenprodil to GluN2B is accompanied by a deceleration of the deactivation kinetics for GluN1/GluN2A or GluN1/GluN2B diheteromers, respectively (Bhatt et al., 2013; Erreger and Traynelis, 2005; Kew et al., 1996; Paoletti et al., 1997; Tovar and Westbrook, 2012). The change in the kinetics of glutamate responses mediated by modulators can modify the temporal characteristics of synaptic integration, which could have physiological and therapeutic relevance. In order to examine the effects of extracellular Zn^{2+} and ifenprodil on the deactivation kinetics, we compared responses to brief (5 ms) glutamate applications in absence of antagonists (control) to responses in the continuous presence of either 1 μ M ifenprodil or 300 nM extracellular Zn^{2+} obtained from the same cell (i.e. paired recordings). The continuous presence of extracellular Zn^{2+} significantly increased $\tau_{weighted}$ of wild type 2A/2A from 33 ± 1 ms (control) to 55 ± 2 ms ($N = 6$; paired t test; two-tailed; $P < 0.05$), whereas ifenprodil did not change the deactivation time course of wild type 2A/2A (Figure 5A,C and Table 2). Inhibition of peak responses by extracellular Zn^{2+} or ifenprodil is shown in Figure 5B. For wild type 2B/2B, ifenprodil significantly increased $\tau_{weighted}$ from 327 ± 17 ms (control) to 490 ± 33 ms ($N = 6$; paired t test; two-tailed; $P < 0.05$), whereas extracellular Zn^{2+} had no effect on the deactivation time course (Figure 5A,E and Table 2). Both in the case of extracellular Zn^{2+} action on wild type 2A/2A and ifenprodil action on wild type 2B/2B, the slower deactivation time course is mediated by an increase in the time constant for the slow component (τ_{slow}) without noticeable changes in the time constant and relative contribution of the fast component (τ_{fast} and % fast) (Table 2).

The presence of ifenprodil resulted in a small, but significant, increase in $\tau_{weighted}$ of 2A_{AC1}/2B_{AC2} triheteromers from 55 ± 3 ms (control) to 60 ± 4 ms ($N = 6$; paired t test; two-

tailed; $P < 0.05$), whereas extracellular Zn^{2+} produced a more pronounced increase to 88 ± 5 ms ($P < 0.05$) (Figure 5A,D and Table 2). Both extracellular Zn^{2+} and ifenprodil slowed the deactivation time course of $2A_{C1}/2B_{AC2}$ triheteromers mainly by increasing the relative contribution of the slow component without changing the time constant of the fast component (τ_{fast}) (Table 2). Thus, the presence of a single GluN2A in the triheteromer has a strong effect on both the glutamate deactivation time course and the capacity of subunit-selective ligands to robustly modify this time course.

Discussion

Despite the widespread interest in NMDA receptors as therapeutic targets, it has not been possible to describe the functional or pharmacological properties of triheteromeric NMDA receptors that are abundantly expressed in the CNS. The main issue preventing discoveries on this front has been related to the problem of expressing a homogenous population triheteromeric receptors in heterologous expression systems. Here, we describe a new approach to overcome this obstacle and reveal features of GluN1/GluN2A/GluN2B triheteromers that can have implications for their role in synaptic transmission as well as for drug discovery. We estimate that the new approach to selectively express GluN1/GluN2A/GluN2B triheteromers at the cell surface using engineered C-terminal peptide tags is highly efficient with $<10\%$ of the total current response mediated by GluN1/GluN2A and GluN1/GluN2B diheteromers. Furthermore, our results demonstrate that the presence of engineered C-terminal peptide tags on GluN2 subunits does not modify NMDA receptor function or pharmacology, thereby enabling stronger conclusions to be drawn from kinetic and mechanistic studies. GluN1/GluN2A/GluN2B is the major subtype in hippocampus and cortex of the adult rodent brain (Al-Hallaq et al., 2007; Luo et al., 1997; Rauner and Kohr, 2011; Sheng et al., 1994; Tovar et al., 2013), but other triheteromeric NMDA receptor subtypes have also been identified in the CNS. GluN1/GluN2B/GluN2D is expressed in cerebellar Golgi cells (Brickley et al., 2003), hippocampal granule cells (Pina-Crespo and Gibb, 2002), and substantia nigra (Jones and Gibb, 2005), whereas GluN1/GluN2A/GluN2C is found in adult cerebellar granule cells (Cathala et al., 2000; Chazot et al., 1994). The approach using engineered peptide tags could potentially enable studies on these other, virtually unexplored, triheteromeric subtypes in heterologous expression systems. However, given the marked diversity in sequence, length, and function of the GluN2 CTDs as well as the greatly varying open probability determined by the GluN2 subunits (Paoletti et al., 2013; Sanz-Clemente et al., 2013; Traynelis et al., 2010), it would likely require optimization of the C-terminal peptide tags as well as the expression system to ensure that only triheteromeric receptors are functionally expressed at the cell surface.

We demonstrate a remarkably fast glutamate deactivation of GluN1/GluN2A/GluN2B triheteromers with a time constant that is 1.8-fold slower than that of GluN1/GluN2A diheteromers, but 5.5-fold faster than that of GluN1/GluN2B diheteromers. This acceleration mediated by the GluN2A subunit is comparable to changes observed for NMDA receptor-mediated excitatory postsynaptic currents (EPSCs) in developing hippocampal and cortical neurons as GluN2A expression increases with age (Flint et al., 1997; Gray et al., 2011; Kirson and Yaari, 1996; Stocca and Vicini, 1998). The strong effect of GluN2A on glutamate deactivation mirrors the pharmacology, since extracellular Zn^{2+} inhibits GluN1/GluN2A/GluN2B triheteromers and GluN1/GluN2A diheteromers with similar potency and efficacy in a manner that appears independent of the GluN2B subunit. By contrast, both potency and efficacy of GluN2B-selective antagonists (ifenprodil and CP-101,606) are markedly reduced at GluN1/GluN2A/GluN2B triheteromers compared to GluN1/GluN2B diheteromers. Extracellular Zn^{2+} also mediate a more pronounced deceleration of glutamate deactivation of triheteromers compared to ifenprodil. The asymmetrical outcome of Zn^{2+} and ifenprodil binding on deactivation of triheteromers nicely matches effects on NMDA

receptor-mediated EPSCs from cultured hippocampal neurons suggested to predominantly express GluN1/GluN2A/GluN2B triheteromers (Tovar et al., 2013; Tovar and Westbrook, 2012). The striking similarities between GluN1/GluN2A/GluN2B triheteromers and GluN1/GluN2A diheteromers with respect to both function and pharmacology could render these subtypes indistinguishable under some experimental conditions and raises the possibility that the contribution of GluN1/GluN2A diheteromers to synaptic physiology is overestimated in some studies.

GluN2A and GluN2B subunits interact with different complements of intracellular proteins, including scaffolding proteins, and their trafficking are differentially regulated in neurons (Sanz-Clemente et al., 2013; Traynelis et al., 2010). GluN2A appears to preferentially reside in synapses, whereas GluN2B can be found both at synaptic and extrasynaptic sites (Bard and Groc, 2011). In addition, it has been elegantly demonstrated that GluN2B possesses endocytotic and recycling motifs in the CTD that dominate sorting of triheteromeric GluN1/GluN2A/GluN2B receptors; a finding that is supported by the observation that GluN2B trafficking is unaffected by the absence of GluN2A expression in GluN2A knock-out mice (Tang et al., 2010). The GluN2A-dependent acceleration of EPSCs that occurs during development has profound effects on the temporal signaling properties and charge transfer, both of which have important consequences for synaptic plasticity. Thus, any triheteromeric NMDA receptor subtype is likely endowed with a unique combination of trafficking and functional properties tailored to meet the requirements at a specific subcellular location or a specific population of cells in the CNS.

The strong influence of GluN2A on glutamate deactivation and pharmacology of GluN1/GluN2A/GluN2B triheteromers suggests asymmetrical contributions of GluN2A and GluN2B to long-range allosteric interactions and conformational states of the receptor. This idea is supported by the significant reduction of the ifenprodil binding rate to triheteromers compared to GluN1/GluN2B diheteromers. Our interpretation of this result is that the GluN2A subunit of GluN1/GluN2A/GluN2B triheteromers influences the ifenprodil binding pocket at the interface between ATDs of GluN1 and GluN2B. This would imply that the orientation or dynamics of the ATDs is different in GluN1/GluN2A/GluN2B triheteromers compared to GluN1/GluN2B diheteromers. The possibility of variation between ifenprodil binding pockets of triheteromers and GluN1/GluN2B diheteromers has important implications for drug discovery, since this difference could be exploited for the development of a new generation of therapeutic agents that selectively target GluN1/GluN2A/GluN2B triheteromers.

In summary, we have provided the first comprehensive assessment of properties relevant for synaptic signaling and therapeutic manipulation of what may be the most abundant NMDA receptor subtype in the adult hippocampus and cortex. In doing this, we developed a new approach to study triheteromeric NMDA receptors, and revealed distinct functional and pharmacological features of GluN1/GluN2A/GluN2B triheteromeric receptors. In the past decade, the focus on triheteromeric NMDA receptors has increased significantly as a growing body of biochemical and anatomical studies has identified triheteromers in most regions of the CNS. The approach and the results described in the present study fill a critical gap in our understanding of glutamate receptors and pave the way for future studies on the role of different triheteromeric NMDA receptor subtypes in normal brain function and disease.

Experimental Procedures

DNA constructs and ligands

Rat cDNAs for GluN1-1a (GenBank accession number U08261; hereafter GluN1), GluN2A (D13211), and GluN2B (U11419) were provided by Drs. S. Heinemann (Salk Institute, La Jolla, CA) and S. Nakanishi (Osaka Bioscience Institute, Osaka, Japan). The cDNA encoding rat GluN2B was modified without changing the amino acid sequence to remove a T7 RNA polymerase termination site located immediately following transmembrane helix M4 (see Supplemental Experimental Procedures). The cDNAs encoding the peptide tags C1 and C2 were custom synthesized (Genscript, Piscataway, NJ) and inserted in place of the stop codon in the open reading frame of GluN2A to generate 2A_{C1} and 2A_{C2} (Figure S1). The CTD of the GluN2B subunit was then replaced by the CTD of the GluN2A subunits 2A_{C1} and 2A_{C2}. Residues 1–844 of resulting chimeric subunits denoted 2B_{AC1} and 2B_{AC2} were identical to GluN2B, and the remaining residues were identical to residues 844–1541 and 844–1533 from 2A_{C1} and 2A_{C2}, respectively. All GluN2 cDNAs were inserted into the pCI-neo vector (Promega, Madison, WI). The pCI-neo vector was used to express GluN1 in *Xenopus* oocytes, whereas the GluN1 cDNA was under the control of the inducible promoter in the pTRE-tight vector for expression in HEK293 Tet-On Advanced cells (Clontech, Mountain View, CA). In addition, cDNA encoding EGFP was inserted between the inducible promoter and the open reading frame of GluN1 (EGFP and GluN1 were not expressed as a fusion protein) in order to reduce expression of GluN1 and obtain a linear relationship between EGFP and GluN1 expression. Amino acids are numbered according to full-length protein, including the signal peptide. See Supplemental Experimental Procedures for full details.

Two-electrode voltage-clamp recordings

Preparation and injection of *Xenopus* oocytes were performed essentially as previously described (Hansen et al., 2013). For experiments using tagged GluN2 subunits, the cRNAs encoding GluN1 as well as C1- and C2-tagged GluN2 were injected at a 1:6:6 ratio at a total volume of 50 nl. For all experiments, the cRNA was diluted with RNase-free water to a concentration that would result in ~10 ng of total injected cRNA. See Supplemental Experimental Procedures for full details.

Whole-cell patch-clamp recordings

HEK293 Tet-On Advanced cells (Clontech, Mountain View, CA) were transfected with plasmid cDNAs encoding GluN1 (together with EGFP in the pTRE-tight vector) and GluN2 subunits at a ratio of 1:2 using the calcium phosphate precipitation method as previously described (Hansen et al., 2013). To minimize cytotoxicity, the culture medium was supplemented with NMDA receptor antagonists D,L-2-amino-5-phosphonovalerate (200 μ M) and 7-chlorokynurenic acid (200 μ M). In addition, 5 ng/ml doxycycline was added to the medium to induce low-level expression of GluN1. Experiments were performed approximately 24 hours following transfection. For experiments on triheteromeric receptors, it was important to only include cells with current responses less than 1000 pA in order to minimize overexpression, which has the potential to circumvent the ER retention signals in the engineered peptide tags. Lower expression levels (i.e. current responses less than 1000 pA) improved the ability of the cell to control trafficking and selectively express triheteromeric receptors at the cell surface. See Supplemental Experimental Procedures for full details.

Supplementary Material

Refer to Web version on PubMed Central for supplementary material.

Acknowledgments

The authors thank A. Tankovic, J. Zhang, and P. Le for excellent technical assistance and T. Nakagawa for helpful discussions. This work was supported by NIH-NINDS grant NS036654, the Villum Kann Rasmussen Foundation, and the Lundbeck Foundation. Stephen F. Traynelis is a co-founder of NeurOp Inc., a pharmaceutical company that is developing NMDA receptor modulators for clinical use.

References

- Al-Hallaq RA, Conrads TP, Veenstra TD, Wenthold RJ. NMDA diheteromeric receptor populations and associated proteins in rat hippocampus. *J Neurosci.* 2007; 27:8334–8343. [PubMed: 17670980]
- Anson LC, Chen PE, Wyllie DJ, Colquhoun D, Schoepfer R. Identification of amino acid residues of the NR2A subunit that control glutamate potency in recombinant NR1/NR2A NMDA receptors. *J Neurosci.* 1998; 18:581–589. [PubMed: 9425000]
- Arai R, Wriggers W, Nishikawa Y, Nagamune T, Fujisawa T. Conformations of variably linked chimeric proteins evaluated by synchrotron X-ray small-angle scattering. *Proteins.* 2004; 57:829–838. [PubMed: 15390267]
- Bard L, Groc L. Glutamate receptor dynamics and protein interaction: lessons from the NMDA receptor. *Mol Cell Neurosci.* 2011; 48:298–307. [PubMed: 21640188]
- Benveniste M, Mayer ML. Kinetic analysis of antagonist action at N-methyl-D-aspartic acid receptors. Two binding sites each for glutamate and glycine. *Biophys J.* 1991; 59:560–573. [PubMed: 1710938]
- Bettini E, Sava A, Griffante C, Carignani C, Buson A, Capelli AM, Negri M, Andretta F, Senar-Sancho SA, Guiral L, et al. Identification and characterization of novel NMDA receptor antagonists selective for NR2A- over NR2B-containing receptors. *J Pharmacol Exp Ther.* 2010; 335:636–644. [PubMed: 20810618]
- Bettler B, Kaupmann K, Mosbacher J, Gassmann M. Molecular structure and physiological functions of GABA(B) receptors. *Physiol Rev.* 2004; 84:835–867. [PubMed: 15269338]
- Bhatt JM, Prakash A, Suryavanshi PS, Dravid SM. Effect of ifenprodil on GluN1/GluN2B N-methyl-D-aspartate receptor gating. *Mol Pharmacol.* 2013; 83:9–21. [PubMed: 23007555]
- Brickley SG, Misra C, Mok MH, Mishina M, Cull-Candy SG. NR2B and NR2D subunits coassemble in cerebellar Golgi cells to form a distinct NMDA receptor subtype restricted to extrasynaptic sites. *J Neurosci.* 2003; 23:4958–4966. [PubMed: 12832518]
- Brock C, Boudier L, Maurel D, Blahos J, Pin JP. Assembly-dependent surface targeting of the heterodimeric GABAB Receptor is controlled by COPI but not 14-3-3. *Mol Biol Cell.* 2005; 16:5572–5578. [PubMed: 16176975]
- Burger PB, Yuan H, Karakas E, Geballe M, Furukawa H, Liotta DC, Snyder JP, Traynelis SF. Mapping the binding of GluN2B-selective N-methyl-D-aspartate receptor negative allosteric modulators. *Mol Pharmacol.* 2012; 82:344–359. [PubMed: 22596351]
- Cathala L, Misra C, Cull-Candy S. Developmental profile of the changing properties of NMDA receptors at cerebellar mossy fiber-granule cell synapses. *J Neurosci.* 2000; 20:5899–5905. [PubMed: 10934236]
- Chazot PL, Coleman SK, Cik M, Stephenson FA. Molecular characterization of N-methyl-D-aspartate receptors expressed in mammalian cells yields evidence for the coexistence of three subunit types within a discrete receptor molecule. *J Biol Chem.* 1994; 269:24403–24409. [PubMed: 7929101]
- Chazot PL, Stephenson FA. Molecular dissection of native mammalian forebrain NMDA receptors containing the NR1 C2 exon: direct demonstration of NMDA receptors comprising NR1, NR2A, and NR2B subunits within the same complex. *J Neurochem.* 1997; 69:2138–2144. [PubMed: 9349560]
- Choi YB, Lipton SA. Identification and mechanism of action of two histidine residues underlying high-affinity Zn²⁺ inhibition of the NMDA receptor. *Neuron.* 1999; 23:171–180. [PubMed: 10402203]
- Clements JD, Westbrook GL. Activation kinetics reveal the number of glutamate and glycine binding sites on the N-methyl-D-aspartate receptor. *Neuron.* 1991; 7:605–613. [PubMed: 1681832]

- Erreger K, Geballe MT, Kristensen A, Chen PE, Hansen KB, Lee CJ, Yuan H, Le P, Lyuboslavsky PN, Micale N, et al. Subunit-Specific Agonist Activity at NR2A-, NR2B-, NR2C-, and NR2D-Containing N-Methyl-D-aspartate Glutamate Receptors. *Mol Pharmacol.* 2007; 72:907–920. [PubMed: 17622578]
- Erreger K, Traynelis SF. Allosteric interaction between zinc and glutamate binding domains on NR2A causes desensitization of NMDA receptors. *J Physiol.* 2005; 569:381–393. [PubMed: 16166158]
- Erreger K, Traynelis SF. Zinc inhibition of rat NR1/NR2A N-methyl-D-aspartate receptors. *J Physiol.* 2008; 586:763–778. [PubMed: 18048453]
- Flint AC, Maisch US, Weishaupt JH, Kriegstein AR, Monyer H. NR2A subunit expression shortens NMDA receptor synaptic currents in developing neocortex. *J Neurosci.* 1997; 17:2469–2476. [PubMed: 9065507]
- Gray JA, Shi Y, Usui H, During MJ, Sakimura K, Nicoll RA. Distinct modes of AMPA receptor suppression at developing synapses by GluN2A and GluN2B: single-cell NMDA receptor subunit deletion in vivo. *Neuron.* 2011; 71:1085–1101. [PubMed: 21943605]
- Hansen KB, Clausen RP, Bjerrum EJ, Bechmann C, Greenwood JR, Christensen C, Kristensen JL, Egebjerg J, Bräuner-Osborne H. Tweaking Agonist Efficacy at N-Methyl-D-aspartate Receptors by Site-Directed Mutagenesis. *Mol Pharmacol.* 2005; 68:1510–1523. [PubMed: 16131614]
- Hansen KB, Ogden KK, Traynelis SF. Subunit-selective allosteric inhibition of glycine binding to NMDA receptors. *J Neurosci.* 2012; 32:6197–6208. [PubMed: 22553026]
- Hansen KB, Tajima N, Risgaard R, Perszyk RE, Jorgensen L, Vance KM, Ogden KK, Clausen RP, Furukawa H, Traynelis SF. Structural determinants of agonist efficacy at the glutamate binding site of N-methyl-D-aspartate receptors. *Mol Pharmacol.* 2013; 84:114–127. [PubMed: 23625947]
- Hatton CJ, Paoletti P. Modulation of triheteromeric NMDA receptors by N-terminal domain ligands. *Neuron.* 2005; 46:261–274. [PubMed: 15848804]
- Jones S, Gibb AJ. Functional NR2B- and NR2D-containing NMDA receptor channels in rat substantia nigra dopaminergic neurones. *J Physiol.* 2005; 569:209–221. [PubMed: 16141268]
- Kammerer RA, Frank S, Schulthess T, Landwehr R, Lustig A, Engel J. Heterodimerization of a functional GABAB receptor is mediated by parallel coiled-coil alpha-helices. *Biochemistry.* 1999; 38:13263–13269. [PubMed: 10529199]
- Karakas E, Simorowski N, Furukawa H. Structure of the zinc-bound amino-terminal domain of the NMDA receptor NR2B subunit. *EMBO J.* 2009; 28:3910–3920. [PubMed: 19910922]
- Karakas E, Simorowski N, Furukawa H. Subunit arrangement and phenylethanolamine binding in GluN1/GluN2B NMDA receptors. *Nature.* 2011; 475:249–253. [PubMed: 21677647]
- Kew JN, Richards JG, Mutel V, Kemp JA. Developmental changes in NMDA receptor glycine affinity and ifenprodil sensitivity reveal three distinct populations of NMDA receptors in individual rat cortical neurons. *J Neurosci.* 1998; 18:1935–1943. [PubMed: 9482779]
- Kew JN, Trube G, Kemp JA. A novel mechanism of activity-dependent NMDA receptor antagonism describes the effect of ifenprodil in rat cultured cortical neurones. *J Physiol.* 1996; 497(Pt 3):761–772. [PubMed: 9003561]
- Kirson ED, Yaari Y. Synaptic NMDA receptors in developing mouse hippocampal neurones: functional properties and sensitivity to ifenprodil. *J Physiol.* 1996; 497(Pt 2):437–455. [PubMed: 8961186]
- Kniazeff J, Bessis AS, Maurel D, Ansanay H, Prezeau L, Pin JP. Closed state of both binding domains of homodimeric mGlu receptors is required for full activity. *Nat Struct Mol Biol.* 2004; 11:706–713. [PubMed: 15235591]
- Laube B, Hirai H, Sturgess M, Betz H, Kuhse J. Molecular determinants of agonist discrimination by NMDA receptor subunits: analysis of the glutamate binding site on the NR2B subunit. *Neuron.* 1997; 18:493–503. [PubMed: 9115742]
- Lester RA, Clements JD, Westbrook GL, Jahr CE. Channel kinetics determine the time course of NMDA receptor-mediated synaptic currents. *Nature.* 1990; 346:565–567. [PubMed: 1974037]
- Low CM, Zheng F, Lyuboslavsky P, Traynelis SF. Molecular determinants of coordinated proton and zinc inhibition of N-methyl-D-aspartate NR1/NR2A receptors. *Proc Natl Acad Sci U S A.* 2000; 97:11062–11067. [PubMed: 10984504]

- Luo J, Wang Y, Yasuda RP, Dunah AW, Wolfe BB. The majority of N-methyl-D-aspartate receptor complexes in adult rat cerebral cortex contain at least three different subunits (NR1/NR2A/NR2B). *Mol Pharmacol*. 1997; 51:79–86. [PubMed: 9016349]
- Maki BA, Aman TK, Amico-Ruvio SA, Kussius CL, Popescu GK. C-terminal domains of N-methyl-D-aspartic acid receptor modulate unitary channel conductance and gating. *J Biol Chem*. 2012; 287:36071–36080. [PubMed: 22948148]
- Margeta-Mitrovic M, Jan YN, Jan LY. A trafficking checkpoint controls GABA(B) receptor heterodimerization. *Neuron*. 2000; 27:97–106. [PubMed: 10939334]
- Nozaki C, Vergnano AM, Filliol D, Ouagazzal AM, Le Goff A, Carvalho S, Reiss D, Gaveriaux-Ruff C, Neyton J, Paoletti P, et al. Zinc alleviates pain through high-affinity binding to the NMDA receptor NR2A subunit. *Nat Neurosci*. 2011; 14:1017–1022. [PubMed: 21725314]
- Paoletti P, Ascher P, Neyton J. High-affinity zinc inhibition of NMDA NR1-NR2A receptors. *J Neurosci*. 1997; 17:5711–5725. [PubMed: 9221770]
- Paoletti P, Bellone C, Zhou Q. NMDA receptor subunit diversity: impact on receptor properties, synaptic plasticity and disease. *Nat Rev Neurosci*. 2013; 14:383–400. [PubMed: 23686171]
- Paoletti P, Perin-Dureau F, Fayyazuddin A, Le Goff A, Callebaut I, Neyton J. Molecular organization of a zinc binding n-terminal modulatory domain in a NMDA receptor subunit. *Neuron*. 2000; 28:911–925. [PubMed: 11163276]
- Pina-Crespo JC, Gibb AJ. Subtypes of NMDA receptors in new-born rat hippocampal granule cells. *J Physiol*. 2002; 541:41–64. [PubMed: 12015419]
- Preskorn SH, Baker B, Kolluri S, Menniti FS, Krams M, Landen JW. An innovative design to establish proof of concept of the antidepressant effects of the NR2B subunit selective N-methyl-D-aspartate antagonist, CP-101,606, in patients with treatment-refractory major depressive disorder. *J Clin Psychopharmacol*. 2008; 28:631–637. [PubMed: 19011431]
- Punnakkal P, Jendritza P, Kohr G. Influence of the intracellular GluN2 C-terminal domain on NMDA receptor function. *Neuropharmacology*. 2012; 62:1985–1992. [PubMed: 22245680]
- Rachline J, Perin-Dureau F, Le Goff A, Neyton J, Paoletti P. The micromolar zinc-binding domain on the NMDA receptor subunit NR2B. *J Neurosci*. 2005; 25:308–317. [PubMed: 15647474]
- Rauner C, Kohr G. Triheteromeric NR1/NR2A/NR2B receptors constitute the major N-methyl-D-aspartate receptor population in adult hippocampal synapses. *J Biol Chem*. 2011; 286:7558–7566. [PubMed: 21190942]
- Sanz-Clemente A, Nicoll RA, Roche KW. Diversity in NMDA receptor composition: many regulators, many consequences. *Neuroscientist*. 2013; 19:62–75. [PubMed: 22343826]
- Sensi SL, Paoletti P, Koh JY, Aizenman E, Bush AI, Hershfinkel M. The neurophysiology and pathology of brain zinc. *J Neurosci*. 2011; 31:16076–16085. [PubMed: 22072659]
- Sheng M, Cummings J, Roldan LA, Jan YN, Jan LY. Changing subunit composition of heteromeric NMDA receptors during development of rat cortex. *Nature*. 1994; 368:144–147. [PubMed: 8139656]
- Stocca G, Vicini S. Increased contribution of NR2A subunit to synaptic NMDA receptors in developing rat cortical neurons. *J Physiol*. 1998; 507(Pt 1):13–24. [PubMed: 9490809]
- Tang TT, Badger JD 2nd, Roche PA, Roche KW. Novel approach to probe subunit-specific contributions to N-methyl-D-aspartate (NMDA) receptor trafficking reveals a dominant role for NR2B in receptor recycling. *J Biol Chem*. 2010; 285:20975–20981. [PubMed: 20427279]
- Tovar KR, McGinley MJ, Westbrook GL. Triheteromeric NMDA receptors at hippocampal synapses. *J Neurosci*. 2013; 33:9150–9160. [PubMed: 23699525]
- Tovar KR, Westbrook GL. The incorporation of NMDA receptors with a distinct subunit composition at nascent hippocampal synapses in vitro. *J Neurosci*. 1999; 19:4180–4188. [PubMed: 10234045]
- Tovar KR, Westbrook GL. Amino-terminal ligands prolong NMDA Receptor-mediated EPSCs. *J Neurosci*. 2012; 32:8065–8073. [PubMed: 22674281]
- Traynelis SF, Burgess MF, Zheng F, Lyuboslavsky P, Powers JL. Control of voltage-independent zinc inhibition of NMDA receptors by the NR1 subunit. *J Neurosci*. 1998; 18:6163–6175. [PubMed: 9698310]

- Traynelis SF, Wollmuth LP, McBain CJ, Menniti FS, Vance KM, Ogden KK, Hansen KB, Yuan H, Myers SJ, Dingledine R. Glutamate receptor ion channels: structure, regulation, and function. *Pharmacol Rev.* 2010; 62:405–496. [PubMed: 20716669]
- Vicini S, Wang JF, Li JH, Zhu WJ, Wang YH, Luo JAH, Wolfe BB, Grayson DR. Functional and pharmacological differences between recombinant N-methyl-D-aspartate receptors. *J Neurophysiol.* 1998; 79:555–566. [PubMed: 9463421]
- Williams K. Separating dual effects of zinc at recombinant N-methyl-D-aspartate receptors. *Neurosci Lett.* 1996; 215:9–12. [PubMed: 8880741]
- Zerangue N, Malan MJ, Fried SR, Dazin PF, Jan YN, Jan LY, Schwappach B. Analysis of endoplasmic reticulum trafficking signals by combinatorial screening in mammalian cells. *Proc Natl Acad Sci U S A.* 2001; 98:2431–2436. [PubMed: 11226256]

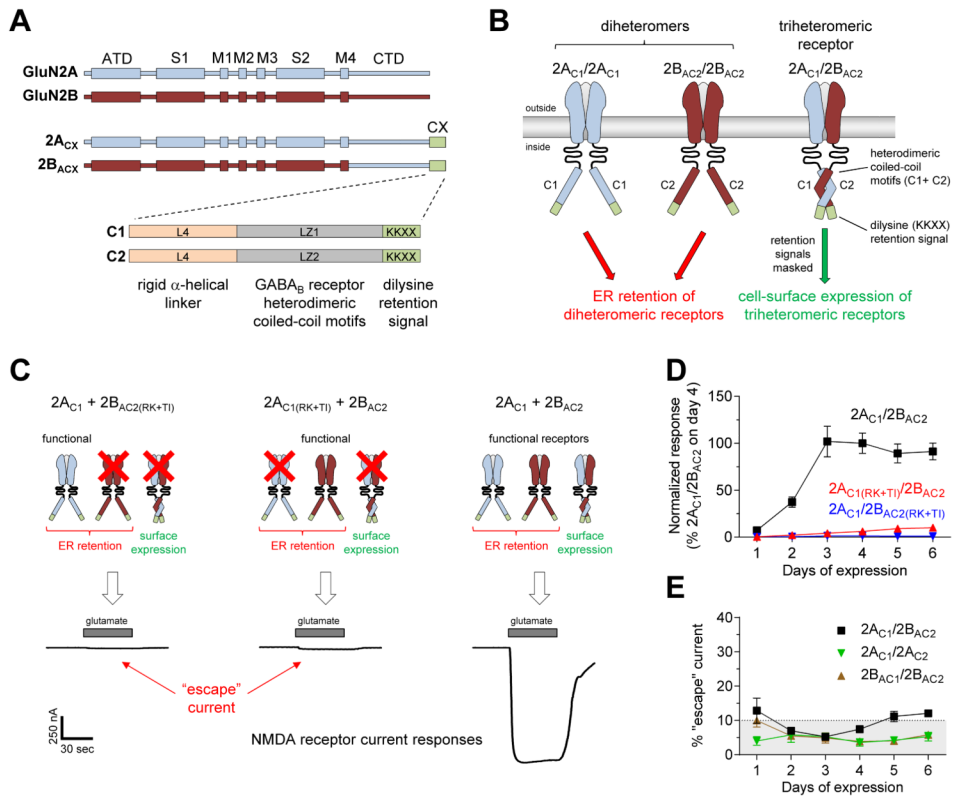
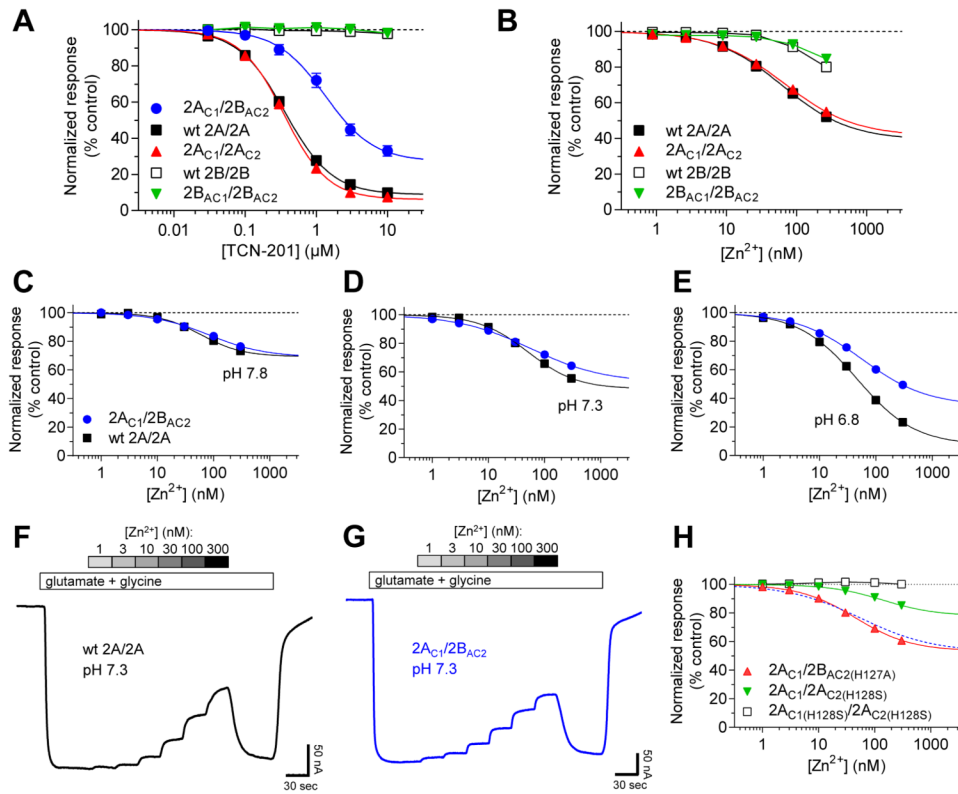
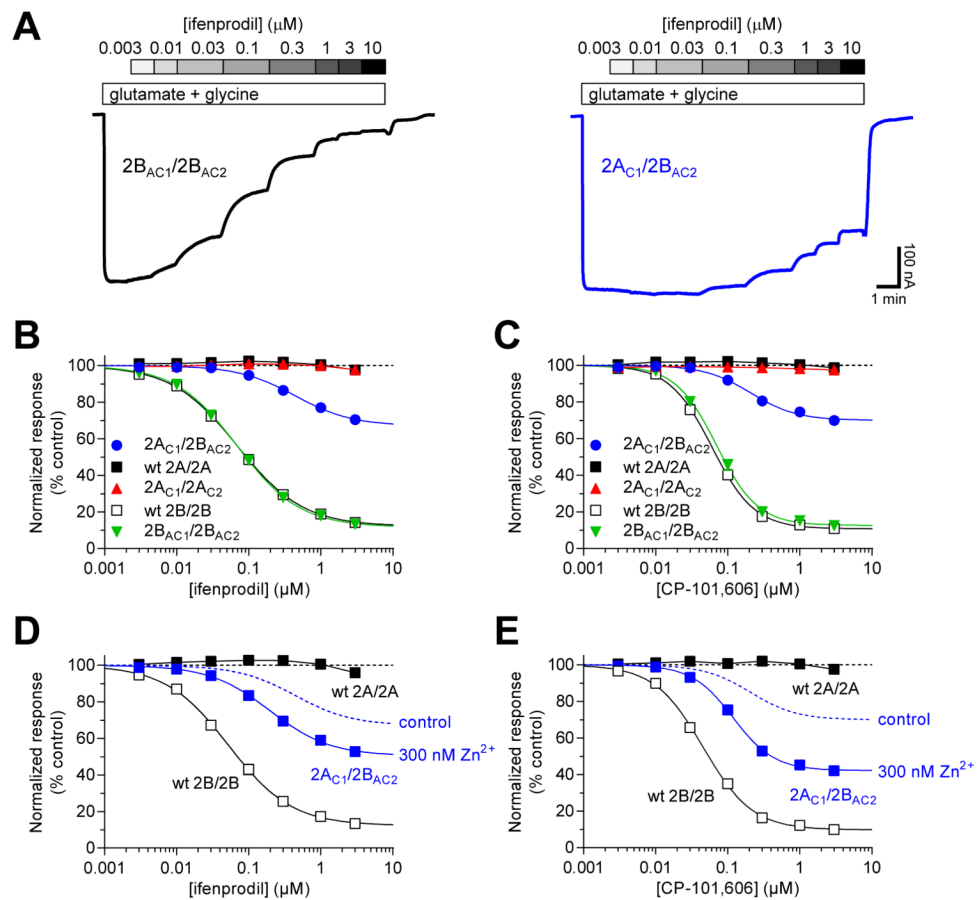


Figure 1. Control of NMDA receptor composition using engineered peptide tags. **(A)** Linear representations of polypeptide chains show the amino terminal domain (*ATD*), S1 and S2 segments of the agonist binding domain, transmembrane helices (*M1*, *M3*, and *M4*), and the reentrant pore loop (*M2*) of GluN2A, GluN2B, GluN2A with C1- or C2-tags fused to the intracellular C-terminus ($2A_{CX}$), and chimeric GluN2B subunits with the C-terminal domain replaced by that of C1- or C2-tagged GluN2A ($2B_{ACX}$). **(B)** Co-expression of GluN1 (omitted from cartoon for clarity) with two different GluN2 subunits in heterologous systems would normally generate three populations of functional NMDA receptors. However, fusing the C1 and C2 tags to the intracellular C-termini of GluN2 subunits should not allow cell-surface expression of receptors that contain two C1-tagged or two C2-tagged GluN2 subunits. **(C)** Representative two-electrode voltage-clamp recordings of responses from recombinant NMDA receptors expressed in *Xenopus* oocytes activated by 100 μ M glutamate plus 50 μ M glycine. GluN1 was co-expressed with either $2A_{C1}$ and mutated $2B_{AC2}$ (R519K + T691I in $2B_{AC2(RK+TI)}$), mutated $2A_{C1}$ (R518K + T690I in $2A_{C1(RK+TI)}$) and $2B_{AC2}$, or $2A_{C1}$ and $2B_{AC2}$. The RK+TI mutations abolish binding of glutamate and render any NMDA receptor containing this subunit non-functional. **(D)** Co-expression of $2A_{C1}$ and $2B_{AC2}$ (as well as GluN1) produced robust currents responses that increased following cRNA injection (*black*), whereas current responses from $2A_{C1}/2A_{C1}$ and $2B_{AC2}/2B_{AC2}$ receptors that may have escaped ER retention remained small. Data are mean \pm SEM and each data point is from 5 batches of oocytes with 6 oocytes for each batch ($N = 30$). **(E)** The sum of the fractional currents assessed using the RK+TI mutations provided an estimate of the percent “escape” current in oocytes co-expressing $2A_{C1}$ and $2B_{AC2}$, $2A_{C1}$ and $2A_{C2}$, or $2B_{AC1}$ and $2B_{AC2}$. See also Figures S1–S3 and Table S1.

**Figure 2.**

Inhibition of triheteromeric receptors by GluN2A-selective antagonists. **(A)** TCN-201 data were generated for wild type receptors (wt $2A/2A$ and wt $2B/2B$) and receptors containing C1- and C2-tagged GluN2 subunits expressed in *Xenopus* oocytes using two-electrode voltage-clamp recordings. Current responses were activated by $100\ \mu\text{M}$ glutamate plus $3\ \mu\text{M}$ glycine. Data are mean \pm SEM from 8–10 oocytes. **(B)** Data for inhibition by extracellular Zn^{2+} were generated for the NMDA receptor subtypes. Current responses were activated by $50\ \mu\text{M}$ glutamate plus $50\ \mu\text{M}$ glycine. Data are from 6–12 oocytes. **(C–E)** Inhibition of wild type GluN1/GluN2A (wt $2A/2A$) and GluN1/GluN2A/GluN2B triheteromers ($2A_{C1}/2B_{AC2}$) by extracellular Zn^{2+} was compared at pH 7.8, 7.3, and 6.8. Data are from 6–28 oocytes. **(F,G)** The representative recordings show inhibition by extracellular Zn^{2+} at physiological pH 7.3. **(H)** Data for inhibition by extracellular Zn^{2+} at physiological pH 7.3 of receptors with a mutation in a single or both Zn^{2+} binding sites (H128S in GluN2A and H127A in GluN2B). The blue dashed line represents the fit of actual data from $2A_{C1}/2B_{AC2}$ shown in panel D. Data are from 6–11 oocytes. See also Table 1 and Figure S4.

**Figure 3.**

Inhibition of triheteromeric receptors by GluN2B-selective antagonists. **(A)** The representative two-electrode-voltage-clamp recordings show ifenprodil inhibition of $2B_{AC1}/2B_{AC2}$ diheteromers and $2A_{C1}/2B_{AC2}$ triheteromers expressed in *Xenopus* oocytes. Current responses were activated by $100 \mu\text{M}$ glutamate plus $50 \mu\text{M}$ glycine. **(B)** Data for ifenprodil inhibition were generated for the NMDA receptor subtypes. Data are mean \pm SEM from 6–16 oocytes. **(C)** Data for CP-101,606 inhibition were generated for the NMDA receptor subtypes. Data are from 7–10 oocytes. **(D,E)** Data for ifenprodil and CP-101,606 inhibition were generated in the continuous presence of 300 nM extracellular Zn^{2+} . The blue dashed lines represents fits of actual data from $2A_{C1}/2B_{AC2}$ (control) generated in the absence of extracellular Zn^{2+} as shown in panels B and C. Data are from 6–8 oocytes. See also Table 1 and Figures S4–S5.

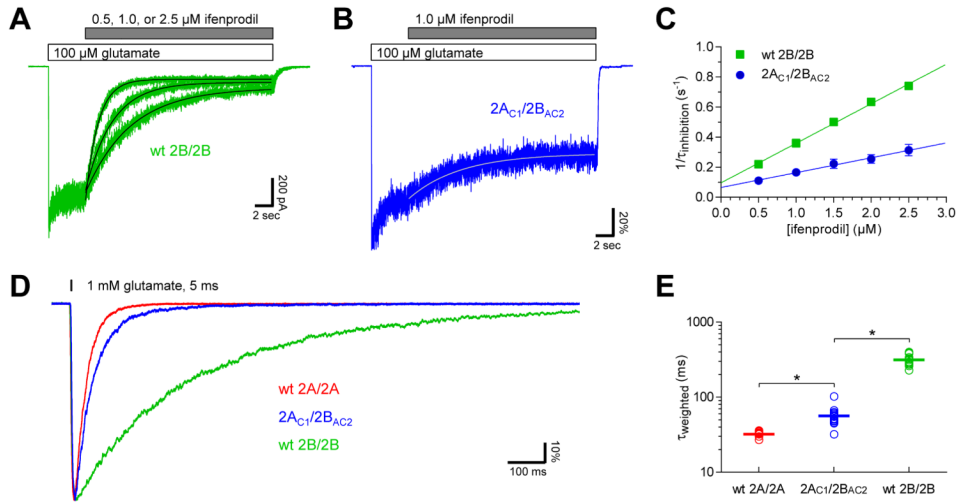


Figure 4. Deactivation time course of triheteromers and rate of ifenprodil inhibition. **(A)** The overlay compares representative whole-cell patch-clamp recordings of current responses from wild type GluN1/GluN2B (wt 2B/2B) expressed in HEK293 cells. The receptors are activated by 100 μM glutamate in the continuous presence of 100 μM glycine. The time course of ifenprodil inhibition of steady-state responses can be described using mono-exponential fits (*black lines*). **(B)** Representative response from GluN1/GluN2A/GluN2B triheteromers ($2A_{C1}/2B_{AC2}$) activated by 100 μM glutamate in the continuous presence of 100 μM glycine and inhibited by ifenprodil. **(C)** The rate of ifenprodil inhibition ($1/\tau_{\text{inhibition}}$) was linearly related to the concentration of ifenprodil, and the slope of the linear fit provides the rate of ifenprodil binding (k_{on}), which was $0.263 \mu\text{M}^{-1}\cdot\text{s}^{-1}$ for wild type 2B/2B ($N = 6$) and $0.099 \mu\text{M}^{-1}\cdot\text{s}^{-1}$ for $2A_{C1}/2B_{AC2}$ triheteromers ($N = 6$). Data are mean \pm SEM. **(D)** The overlay compares representative whole-cell patch-clamp recordings of responses normalized to the peak amplitude. The diheteromeric wt 2A/2A and 2B/2B and triheteromeric $2A_{C1}/2B_{AC2}$ receptors were expressed in HEK293 cells and activated by brief pulses (5 ms) of 1 mM glutamate in the continuous presence of 100 μM glycine. **(E)** The graph plots the weighted time constants for deactivation following removal of glutamate from individual cells (*circles*) as well as the mean (*horizontal line*) for wild type 2A/2A ($N = 11$), $2A_{C1}/2B_{AC2}$ triheteromers ($N = 17$), and wild type 2B/2B ($N = 15$). * denotes significantly different (unpaired t test; two-tailed, $P < 0.05$). See also Table 2, Figure S6, and Table S2.

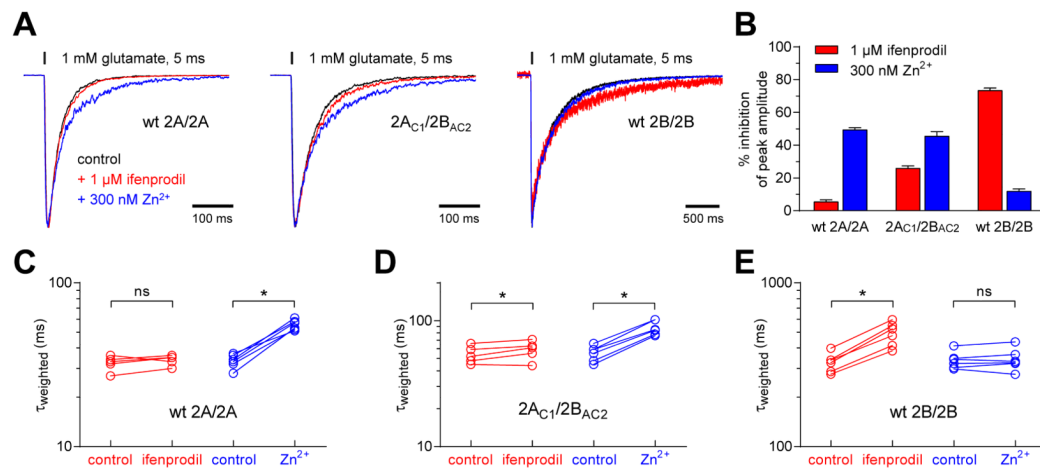


Figure 5.

Effects of extracellular Zn^{2+} and ifenprodil on deactivation time course. (A) The overlay compares representative whole-cell patch-clamp recordings of current responses normalized to the peak amplitude from wild type 2A/2A (left), 2A_{C1}/2B_{AC2} triheteromers (middle), and wild type 2B/2B (right) expressed in HEK293 cells. The receptors were activated by brief pulses (5 ms) of 1 mM glutamate in the absence (control; black line) or presence of 1 μM ifenprodil (red line) or 300 nM extracellular Zn^{2+} (blue line). Glycine (100 μM) was present at all times. (B) The bar graph shows the percent inhibition of the peak amplitude by ifenprodil or extracellular Zn^{2+} relative to control. Each bar represents mean \pm SEM from 6 cells. (C–E) The graphs plot the weighted time constants of individual cells expressing wild type 2A/2A, 2B/2B, and 2A_{C1}/2B_{AC2} triheteromers. Responses to brief (5 ms) glutamate applications in absence of antagonists (control) were compared to responses in the presence of either 1 μM ifenprodil or 300 nM extracellular Zn^{2+} obtained from the same cell (i.e. paired recordings). * denotes significantly different (paired t test; two-tailed, $P < 0.05$), and ns indicates not significant. See also Table 2.

Glutamate deactivation time course of NMDA receptors. NMDA receptors expressed in HEK293 cells were activated by brief application (5 ms) of 1 mM glutamate in the continuous presence of 100 μ M glycine and recorded using whole-cell patch-clamp electrophysiology. Responses were activated in the absence (control) or presence of either 1 μ M ifenprodil or 300 nM extracellular Zn^{2+} . Deactivation time courses were described using dual-exponential fits to obtain τ_{fast} and τ_{slow} , and % fast is the fitted percentage of the fast component. Weighted time constants ($\tau_{weighted}$) were calculated as described in Table S2. Control $\tau_{weighted}$ were compared using unpaired t test (two-tailed), and * or # indicates significantly different from control at wild type 2A/2A or 2B/2B, respectively ($P < 0.05$). Control $\tau_{weighted}$ were also compared to $\tau_{weighted}$ obtained in the presence of ifenprodil or extracellular Zn^{2+} for the same cell using paired t test (two-tailed), and § indicates significantly different from control ($P < 0.05$). N is the number of cells and all values are mean \pm SEM. See also Figure S6 and Table S2.

Table 2

GluN2 subunits (co-expressed with GluN1)	Brief glutamate activation (5 ms)					
	τ_{fast} (ms)	τ_{slow} (ms)	% fast	$\tau_{weighted}$ (ms)	N	
wt 2A/2A	control	30 \pm 1	95 \pm 21	78 \pm 7	32 \pm 1 [#]	11
	+ ifenprodil	30 \pm 1	90 \pm 23	77 \pm 9	34 \pm 1	6
	+ Zn^{2+}	28 \pm 1	130 \pm 14	72 \pm 2	55 \pm 2 [§]	6
2A_{AC1}/2A_{AC2}	control	29 \pm 1	102 \pm 46	76 \pm 9	33 \pm 2 [#]	6
	control	152 \pm 12	496 \pm 19	52 \pm 2	314 \pm 13 [*]	15
wt 2B/2B	+ ifenprodil	157 \pm 9	907 \pm 81	55 \pm 2	490 \pm 33 [§]	6
	+ Zn^{2+}	147 \pm 16	510 \pm 27	46 \pm 3	343 \pm 22	6
	control	109 \pm 13	422 \pm 34	47 \pm 8	274 \pm 24 [*]	4
2B_{AC1}/2B_{AC2}	control	39 \pm 3	146 \pm 16	79 \pm 4	57 \pm 4 ^{*#}	17
	+ ifenprodil	39 \pm 4	118 \pm 19	66 \pm 8	59 \pm 4 [§]	6
2A_{AC1}/2B_{AC2}	+ Zn^{2+}	39 \pm 5	153 \pm 10	57 \pm 3	88 \pm 5 [§]	6